

Nanotexturing To Enhance Photoluminescent Response of Atomically Thin Indium Selenide with Highly Tunable Band Gap

Mauro Brotons-Gisbert,[†] Daniel Andres-Penares,[†] Joonki Suh,[‡] Francisco Hidalgo,[§] Rafael Abargues,^{||} Pedro J. Rodríguez-Cantó,^{||} Alfredo Segura,[†] Ana Cros,[†] Gerard Tobias,[⊥] Enric Canadell,[⊥] Pablo Ordejón,[§] Junqiao Wu,[‡] Juan P. Martínez-Pastor,^{*,†} and Juan F. Sánchez-Royo^{*,†}

[†]ICMUV, Instituto de Ciencia de Materiales, Universidad de Valencia, P.O. Box 22085, 46071 Valencia, Spain

[‡]Department of Materials Science and Engineering, University of California, Berkeley, California 94720, United States

[§]Catalan Institute of Nanoscience and Nanotechnology (ICN2), CSIC and The Barcelona Institute of Science and Technology, Campus UAB, Bellaterra 08193 Barcelona, Spain

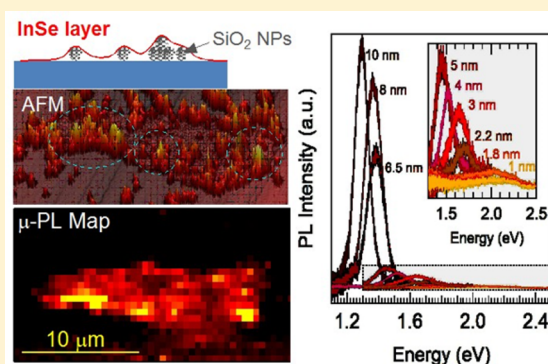
^{||}Intenanomat S.L., c/Catedrático José Beltrán 2, 46980 Paterna, Spain

[⊥]Institut de Ciència de Materials de Barcelona (ICMAB-CSIC), Campus de la UAB, 08193 Bellaterra, Barcelona, Spain

Supporting Information

ABSTRACT: Manipulating properties of matter at the nanoscale is the essence of nanotechnology, which has enabled the realization of quantum dots, nanotubes, metamaterials, and two-dimensional materials with tailored electronic and optical properties. Two-dimensional semiconductors have revealed promising perspectives in nanotechnology. However, the tunability of their physical properties is challenging for semiconductors studied until now. Here we show the ability of morphological manipulation strategies, such as nanotexturing or, at the limit, important surface roughness, to enhance light absorption and the luminescent response of atomically thin indium selenide nanosheets. Besides, quantum-size confinement effects make this two-dimensional semiconductor to exhibit one of the largest band gap tunability ranges observed in a two-dimensional semiconductor: from infrared, in bulk material, to visible wavelengths, at the single layer. These results are relevant for the design of new optoelectronic devices, including heterostructures of two-dimensional materials with optimized band gap functionalities and in-plane heterojunctions with minimal junction defect density.

KEYWORDS: Two-dimensional materials, indium selenide, microphotoluminescence, optical properties, band gap engineering, nanotexturing



Many efforts have been devoted to manipulate the morphology of materials with large surface-to-volume ratio at the nanoscale to control and improve their functionalities. Two-dimensional (2D) materials are especially suitable for nanotexturing with the advantage that physical and mechanical properties converging in them hardly coexist in bulk compounds and have potential applications in nanotechnology.^{1–3} It is usually believed that nanotexturing reduces transport abilities of 2D systems whereas it introduces or enhances other functionalities. That is the case, for instance, of graphene. Ultraflat graphene with reduced substrate interactions has shown a drastic improvement in carrier mobility,^{4,5} with respect to that on SiO₂. Conversely, corrugation enhances graphene functionalities for sensing,⁶ and mechanical structuring has been proposed as a noninvasive strategy to open the long awaited band gap for this material.⁷ Single layers (SLs) of transition-metal dichalcogenides, the first 2D semiconductors that have emerged to complement the zero band gap shortcomings of graphene,^{8–10} offer unquestionable techno-

logical applications as field-effect transistors,^{11,12} photodetectors,^{13,14} and sensors,¹⁵ as well as photovoltaic¹⁶ and valleytronic^{17,18} devices. Nevertheless, tuning their properties for optoelectronic applications is challenging due to the intrinsically localized nature and orbital character of the d-states that dominate their valence and conduction bands.^{9,19} Quantum-size confinement effects achieve the tuning of the band gap of few-layer dichalcogenide nanosheets, but only atomically thin dichalcogenides exhibit important photoluminescence (PL) due to an indirect-to-direct character transition.^{8–10} Furthermore, dipolar selection rules for 2D dichalcogenides favor optical transitions to occur for electric field polarized in the layer plane,²⁰ and luminescent recombination originates solely from in-plane excitons.²¹ As a

Received: February 17, 2016

Revised: April 11, 2016

Published: April 15, 2016

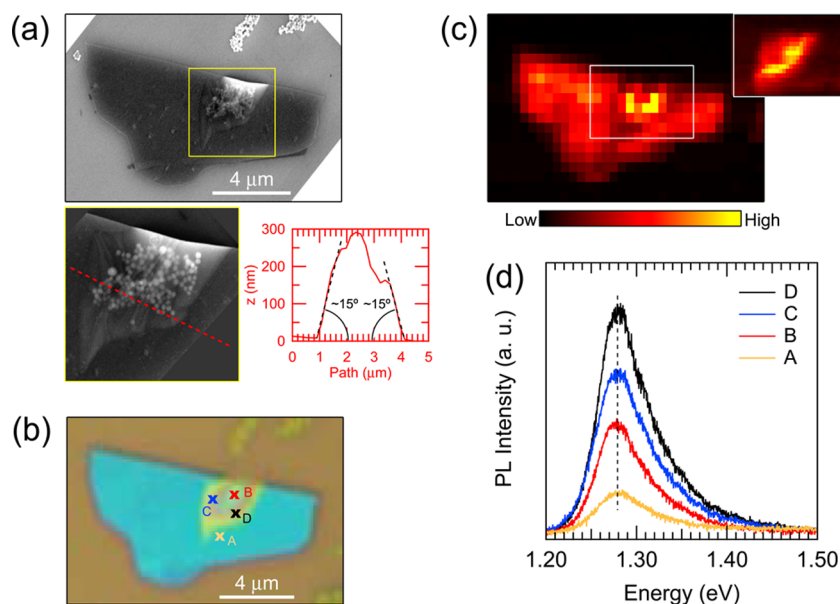


Figure 1. Morphology and luminescent response of lifted up few-layer InSe nanosheets. (a) SEM image obtained in a partially lifted InSe nanosheet of 12 nm in thickness, as determined by AFM. A detailed SEM image of the lifted region of the nanosheet—the one delimited by a yellow rectangle—can be seen at the bottom of the main SEM image. The AFM contour shown at the bottom-right side was obtained from the nanosheet along the path marked on the detailed SEM image by a red dashed line. The deflection angles of the microramps of the lifted region are indicated in the AFM profile. (b) Optical image of this InSe nanosheet. Notice the bright region in the nanosheet image, which reveals the presence of trapped NPs. All images have been similarly rotated for ease of comparison. (c) Integrated-PL intensity map measured in this InSe nanosheet. The integration was performed in the 1.2–1.5 eV range. The PL map was acquired with steps of 0.5 μm . Intensity values are represented by the color-code bar shown at the bottom of the map. The inset shows the integrated-PL intensity map measured in the region delimited by the white rectangle depicted in the main PL-map. This detailed PL-map was acquired with steps of 0.2 μm . (d) Micro-PL spectra measured in selected points of the nanosheet, which correspond to the points labeled from A to D in the optical image of part b. The vertical dashed line indicates the position of the PL-peak maximum, which appears at 1.279 ± 0.001 in all of the spectra.

consequence, useful morphological manipulation of 2D dichalcogenides was mainly restricted to external forces such as strain. Under large uniaxial strain, the band gap of MoS_2 has appeared to diminish by 0.1 eV,²² which was the basis to confer artificial atom characteristics to this nanomaterial with enhanced PL due to exciton funneling.²³

Few layered semiconductors have valence and conduction bands coming from more delocalized s- and p-orbitals. Indium selenide (InSe), a layered semiconductor of the III–VI family with a direct band gap of ~ 1.25 eV at room temperature,²⁴ is one of these exceptions since its lowermost conduction band basically stems from antibonding In s states, whereas its uppermost valence band has a nonbonding Se p_z character.²⁵ On top of these electronic properties, InSe is exfoliable²⁶ and chemically stable,²⁷ presents the highest electron mobility among layered semiconductors ($\sim 10^5$ $\text{cm}^2 \text{V}^{-1} \text{s}^{-1}$ at room temperature),²⁸ and has an anomalous electron effective-mass anisotropy ($m_{e,\parallel c}^*/m_{e,\perp c}^* = 0.081/0.138$, where the c -axis is perpendicular to the layer plane).²⁹ Bulk InSe has also applications in photovoltaics,^{30–32} Li-ion batteries,³³ and thermoelectricity.³⁴ The confluence in a single material of such characteristics and applicability allows to envisage 2D InSe to become a very versatile material for electronics and optoelectronics with tunable and optimized functionalities. In fact, first-principles calculations predicted that 2D InSe should produce a band gap tuning window as large as ~ 1.1 eV,³⁵ and experimentally, a blue shift of the optical band gap of 0.2 eV has been already observed in 5 nm thick InSe nanosheets at low and high temperatures.^{35,36} Also, devices based on few-layer InSe have shown promising applications, such as image sensors,³⁷ field-effect transistors with bulk-like mobilities³⁸

and large current on–off ratios ($\sim 10^8$),³⁹ and photodetectors with high performance capabilities.^{40–43} Nevertheless, such a potentially wide band gap tunability has not been demonstrated yet, probably due to the poor emission intensity measured in InSe nanosheets.^{35,36} In this work we achieve two important milestones for future applications of 2D InSe semiconductors in electronics and optoelectronics/photronics. First of all, we propose a nanotexturing strategy to enhance the room temperature light emission intensity in few-layer and SL InSe, by taking advantage of their large optical anisotropy—the dipole matrix elements for light polarization parallel to the c -axis ($\vec{E} \parallel c$) are nearly 2 orders of magnitude larger than those for the perpendicular case ($\vec{E} \perp c$)—. Nanosheets were locally textured by the presence of SiO_2 nanoparticle (NP) agglomerates deposited on a standard Si/ SiO_2 substrate. In the textured areas, a large proportion of light absorbed or emitted perpendicular to the substrate is polarized parallel to the nanosheet c -axis, which enhances both absorption and emission. Second, we demonstrate an optical band gap tuning of near 1 eV from bulk to single layer InSe; i.e., the absorption band-edge increases from 1.25 (infrared) to 2.1 eV (visible), which is one of the largest optical windows observed so far in the bulk-to-SL transition of a given semiconductor and comparable to that observed in phosphorene.⁴⁴

The morphology of few-layer InSe nanosheets has an important influence on their luminescence response. Previous to the deposition of exfoliated nanosheets on SiO_2/Si substrates, SiO_2 NPs of ~ 100 nm in diameter were dispersed on the substrates, in a density high enough to favor the formation of agglomerates of some hundreds of nanometers in

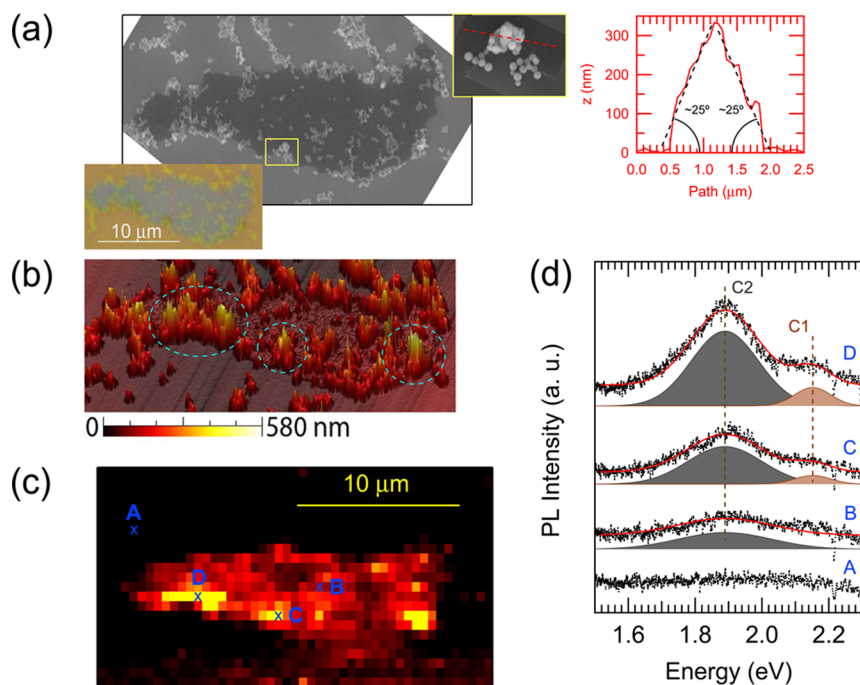


Figure 2. Morphology and luminescent response of textured atomically thin InSe nanosheets. (a) SEM and optical images obtained in a highly textured atomically thin InSe nanosheet. The top-right inset shows a detailed SEM image taken at the border of the nanosheet corresponding to the yellow rectangle depicted on the main SEM image. The AFM contour shown at the right side was obtained from the nanosheet along the path indicated on the detailed SEM image by a red dashed line. This AFM contour evidences nanosheet deflection angles as high as 25 degrees. (b) Perspective of the morphology of the nanosheet, as obtained by AFM. AFM heights are represented by the color-code bar shown at the bottom. Highly textured regions of the nanosheet have been indicated by dashed conic sections. (c) Integrated-PL intensity map measured in this nanosheet. The integration was performed in the 1.5–2.3 eV range. The PL-map was acquired with steps of $0.5 \mu\text{m}$ and follows the same color-code as that of Figure 1c. Notice the correspondence between the three highly textured regions of the nanosheet (b) and the spots with an enhanced PL signal. (d) Micro-PL spectra acquired in selected points of the substrate and the nanosheet, which correspond to the points labeled as A (substrate) and B to D (nanosheet) in the map of Figure 2c. Gaussian deconvolution of the PL spectra allows resolving at least two components, those labeled as C1 and C2 and located at 2.15 ± 0.02 and 1.89 ± 0.01 eV, respectively. The results of the deconvolution process are shown under each particular spectrum. The position of the C1 and C2 components is indicated by vertical dashed bars.

height (several stacked NPs), but sparse throughout the substrate surface due to the spin-coating of the NP solution at sufficiently high angular velocity. On these NP agglomerates, mechanically exfoliated few-layer InSe nanosheets were deposited, as the 12 nm thick one shown in Figure 1a. Optically (Figure 1b), the presence of SiO_2 NPs enhances light scattering, and consequently nanosheets trapping them underneath experience strong color contrast changes. This optical hallmark makes it possible to easily identify such nanosheets among those lying on the bare regions of the SiO_2/Si substrate, even when few NPs become trapped (see Figure S1 of the Supporting Information). The nanosheet shown in Figure 1a and b can be considered an archetype of the few-layer sheets obtained. As we observed by scanning electron microscopy (SEM), NPs agglomerates locally lift up nanosheets. The lifted nanosheets wrap the NP agglomerates—free from microfractures—and evolve as microramps at their edges (Figure 1a). The characteristics of these microramps are intrinsic to the lifting process, since these microramps naturally appear to balance the sheet-substrate adhesion force and the intrinsic elastic strain of the sheets. Interestingly, the average deflection angle of these microramps appears to be of the order of $10\text{--}20^\circ$ (Figure 1a), as measured by atomic force microscope (AFM), which envisages a robust and flexible elastic property of InSe nanosheets since these deflection angles are comparable to those observed in atomically thin MoS_2 sheets just before fracture.⁴⁵

To reveal the effects of morphological manipulation on the luminescent response of few layer InSe, we show in Figure 1c the integrated-PL intensity map measured by micro-PL ($\mu\text{-PL}$) in the InSe nanosheet depicted in Figure 1b. The obtained PL intensity map evidences a homogeneous distribution over the whole nanosheet except at the part of the sample corresponding to its lifted region, where the integrated-PL intensity is clearly enhanced. More precisely, a high-resolution integrated-PL intensity map measured in the lifted zone (inset of Figure 1c) seems to indicate that the most intense PL signal stems from the microramps of the lifted region, rather than its top. In order to confirm this, Figure 1d shows the $\mu\text{-PL}$ spectra recorded in selected points of the nanosheet that correspond to those marked on the image of Figure 1b. The $\mu\text{-PL}$ spectra acquired in points of the flat region of the InSe nanosheet (as the A-point) show a peak at 1.279 ± 0.001 eV which is attributable to the band-to-band transition that is blueshifted by 30 meV with respect to that of bulk InSe due to quantum-size confinement effects of the natural quantum-well determined by a few layer InSe sheet.³⁶ In the lifted region, the PL peak is observed at the same energy position, although it experiences a notable intensity enhancement at the top of the lifted region (B-point) and even higher in points located at the microramp (a factor 5 at the D-point). Figure S1 of the Supporting Information provides similar results obtained in a ~ 4 nm thick InSe nanosheet.

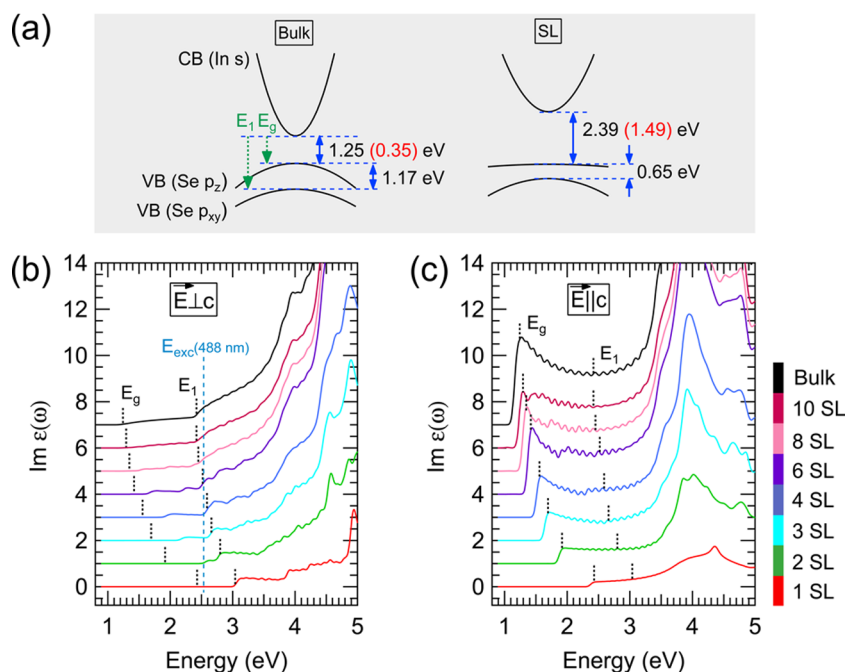


Figure 3. Optical properties of 2D InSe nanosheets. (a) Scheme of the conduction and valence bands of bulk InSe and its SL, as extracted from ref 35. The band gap values obtained by density functional theory are indicated in red colors, whereas those in black take into account their usual band gap underestimation. The band gap of bulk InSe at room temperature—1.25 eV—has been used as a reference value. The two first optical transitions expected to occur in InSe have been labeled as E_g and E_1 , respectively. (b and c) Imaginary part of the dielectric function calculated for InSe nanosheets when the electric field is polarized perpendicular and parallel to the c -axis, respectively. Each curve corresponds to an InSe slab whose thickness is indicated by the color code plotted at the right side of the figure. For the sake of comparison with experimental results, the $Im \epsilon(\omega)$ curves have been rigidly shifted in energy by 0.9 eV, to take into account the well-known underestimation of absolute band gap values as calculated by density functional theory.³⁵ The positions expected for the E_g and E_1 optical transitions for each nanosheet thickness have been indicated by small vertical dashed lines, as obtained from ref 35. In part b, the energy of the excitation light used for the experiments summarized in Figure 4 has been indicated by a vertical dashed line.

The above presented results suggest that morphological manipulation strategies, such as nanotexturing or induced roughness, can enhance the optical performance not only of slabs of few layers of InSe but also of atomically thin nanosheets. This possibility is crucial to pave the way for the potential optoelectronic applications of atomically thin InSe, since the band gap of 2D InSe has been predicted to vary over a broad window as large as 1.1 eV when the InSe thickness decreases until the SL limit.³⁵ However, in practice, the luminescent response of nanosheets thinner than 5 nm suffers from a strong quenching.³⁶ Conditions to obtain textured nanosheets were favored by controlling the NP dispersion process on SiO_2/Si substrates in order to reduce NP agglomeration and favor their dispersion. Figure 2a shows SEM and optical images of an InSe nanosheet exfoliated on a dense distribution of NPs whose thickness d is less than 2 nm, insofar optical contrast techniques can be used for thickness determination of textured InSe nanosheets.²⁶ The high roughness degree caused by the distribution of NPs prevents a precise determination of d by AFM. In fact, the AFM profiles obtained at nanosheet edges far from the NPs give heights of 30 nm, which suggests that most of the sample is adhered on top of the NP agglomerates. In spite of this, the morphology map of this sample shown in Figure 2b, as measured by AFM, reveals a high texturization degree in the nanosheet, in which some points—indicated by dashed conic sections—exhibit deflection angles as high as 20–30° (Figure 2a). The effects of texturization on the luminescent response of this atomically thin nanosheet can be clearly observed in the measured

integrated-PL intensity map (Figure 2c), in which a clear correspondence can be established between points of the nanosheet with enhanced PL signal and those being highly texturized (Figure 2b). The μ -PL spectra shown in Figure 2d, which were acquired in the selected points of the substrate and the nanosheet that are marked in Figure 2c (A and B–D points, respectively), indicate that the PL signal of the flattest parts of the nanosheet can be described by a single peak (labeled as C2) centered at 1.89 ± 0.01 eV, that is, shifted by 0.64 eV from that of the bulk and hence lying at the visible spectrum. Furthermore, the intensity enhancement of the μ -PL spectra produced in texturized regions of the nanosheet (in particular, at the C- and D-points) allows to resolve the existence of an additional PL peak, labeled as C1, located at even higher energies, at 2.15 ± 0.02 eV, besides of the C2 peak whose intensity is enhanced by a factor 3 with respect to that at the flattest region of the nanosheet.

The demonstrated ability of nanotexturing strategies to enhance the luminescence response of 2D InSe can be explained by the combined effect of light scattering by the SiO_2 NPs and NP agglomerates trapped under the nanosheets and the inherent anisotropy of light–matter interactions in 2D InSe. In 2D dichalcogenides, the existence of strong peaks in the joint density of states associated with Van Hove singularities gives rise to strong light absorption in the visible range¹ when the electric field is polarized in the layer plane.²⁰ InSe nanosheets present a notable joint density of states accessible for optical transitions at the high energy side of the visible spectrum (see Figure S2 of the Supporting Information).

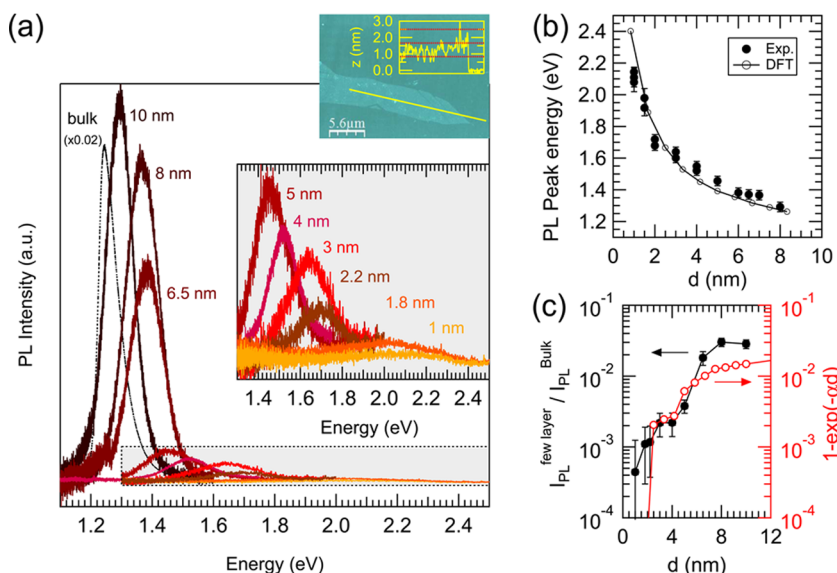


Figure 4. Quantum-confinement effects on the optical properties of 2D InSe nanosheets. (a) Micro-PL spectra acquired in InSe nanosheets exfoliated on bare SiO₂/Si substrates. The thickness of the InSe nanosheet is indicated on each spectrum. As shown in the top inset, the probed nanosheets were as thin as 1 nm, as determined by AFM. The inset at the middle of the plot is a zoom of the gray-shaded rectangle indicated on the main plot. (b) Nanosheet-thickness dependence of the PL-peak maximum of the spectra shown in part a. In this plot we have included results from other measurements performed, for statistics purposes. Error bars are obtained from Gaussian fits of the experimental spectra. As a comparison, the thickness dependence of the band gap of InSe has been included, as obtained by density functional theory,³⁵ taking into account that the bulk band gap is 1.25 eV at room temperature and the nominal InSe SL thickness is 0.833 nm. (c) Nanosheet-thickness dependence of the PL-peak integrated intensity of the spectra shown in Figure 4a. The PL-peak integrated-intensity values have been normalized, for convenience, to that of the spectrum acquired in a bulk-like slab (40 nm thick), which is also shown in a. The thickness dependence of the light absorption ratio has been also included, which has been calculated by considering the thickness dependence of the $Im \epsilon(\omega)$ for $\vec{E} \perp c$ at the excitation energy of 2.54 eV, which can be obtained from data shown in Figure 3b.

However, dipolar selection rules for optical transitions in 2D InSe are just the opposite of those for 2D dichalcogenides. InSe belongs to the C_{3v} point group, in whose symmetry the first band-to-band optical transition (labeled as E_g in Figure 3a) is forbidden for $\vec{E} \perp c$ as both the valence band maximum (with Se-p_z character) and the conduction band minimum (with In-s character) belong to the A₁ representation. Spin-orbit interaction makes it weakly allowed by mixing with deeper lying valence bands, with Se p_x-p_y character, belonging to the E representation. The optical transition from these deeper valence bands to the conduction band (labeled as E₁ in Figure 3a) is fully allowed. The imaginary part of the dielectric function ($Im \epsilon(\omega)$) calculated by using already reported first-principles band-structure calculations³⁵ clearly reflects the role of the optical selection rules of 2D InSe. Figure 3b shows the $Im \epsilon(\omega)$ evaluated for $\vec{E} \perp c$ in bulk and nanosheets. The $Im \epsilon(\omega)$ smoothly increases as $(\omega - E_g)^{3/2}$ as soon as $\omega > E_g$ as expected for a forbidden transition, until the allowed E₁-transition is reached. For the case of the InSe SL (D_{3h} point group) the E_g transition is strictly forbidden due to the existence of a symmetry-plane. On the contrary, The $Im \epsilon(\omega)$ calculated for $\vec{E} \parallel c$ in bulk and nanosheets (Figure 3c) shows that the E_g- and E₁-related transitions exchange their roles. These optical dipolar selection rules explain, for instance, that bulk InSe absorption coefficient for $\vec{E} \parallel c$ is as high as that of dichalcogenides for $\vec{E} \perp c$ ($\sim 10^5$ cm⁻¹) at energies corresponding to the visible spectrum.⁴⁶ Also, the described optical anisotropy of InSe appears to be responsible for the enhancement of the intrinsic luminescent response observed in texturized InSe nanosheets and explains why PL is enhanced

in the microramps originated by the texturization. In these microramps, with deflection angles of 10–30° with respect to the substrate plane, the effective absorption coefficient is increased by the field component parallel to the *c*-axis, which, in this tilted configuration, also enhances light emission. In fact, if we perform μ -PL experiments on tilted nanosheets without NPs below we also find a certain enhancement of the PL intensity (see Figure S3 of the Supporting Information), even if smaller than that discussed above. Of course, the presence of SiO₂ NPs trapped under the nanosheets is contributing to enhance light absorption by light scattering, since they appear to mainly favor the light scattering of red and green wavelengths impinging on the lower side of the nanosheets with off-normal incidence angles (see Figure S4 of the Supporting Information). Lifting nanosheets from the SiO₂/Si substrate may have additional effects that could also enhance light emission, such as the modification of the dielectric properties of the surrounding media and the lower probability of surface trapping of excitons as compared to the case of a standard 2D-semiconductor/SiO₂ interface.

Results shown in Figures 1 and 2 point out that InSe nanosheets would exhibit a large band gap tunability range with high absorption and luminescent capabilities by nanotexturing, which naturally raises the question about the magnitude of the tunability range of the band gap of InSe by reducing its thickness. In fact, stacks of solution-processed ultrathin InSe nanosheets, which were chemically synthesized in the presence of organic solvents acting as surface ligands that lead to stable colloids—from which drop casted samples were prepared—exhibit a PL band peaked at ~ 2 eV.⁴⁷ To approach this question, we show in Figure 4a the μ -PL spectra acquired in InSe nanosheets exfoliated on bare SiO₂/Si substrates, having

proved samples as thin as 1 nm thick (inset of Figure 4a), which corresponds to the InSe SL whose nominal thickness is 0.833 nm.⁴⁸ The maximum of the PL-peak measured at each particular nanosheet spreads from 1.25 eV, in nearly bulk nanosheets, to 2.11 eV, in SL ones. The thickness dependence of the exciton optical transition and hence the optical band gap of InSe nanosheets, as obtained from the PL-peak maxima, follows a trend that seems to be nicely described in terms of quantum-size confinement effects on the direct band gap of InSe (Figure 4b), as calculated by first-principles calculations.³⁵ From these results, the C2 and C1 components resolved in the PL spectra of the texturized nanosheet of Figure 2 appear to come from two and one SL domains probed in our measurements, respectively. Therefore, our results reveal that, by quantum-size confinement effects, the band gap of 2D InSe nanosheets can be widely tuned from the infrared, in the bulk, to well inside the visible reaching orange wavelengths, at the SL.

Finally, we would like to approach the question related to the origin of the poor luminescent behavior of flat InSe nanosheets.^{35,36} First-principles calculations have predicted few-layer InSe to convey a band gap blue shift at the same time that the semiconductor turns from direct, in bulk, into pseudoindirect, in few atomic layers.^{35,49} In the pseudoindirect few-layer InSe, the valence band adopts a camel-back-like shape and its maximum appears only few tens of meV above the valence band states at Γ (reported values oscillate between 15³⁵ and 50 meV⁴⁹) where the conduction band minimum is located. The strong quenching of the PL observed in InSe nanosheets as d decreases^{35,36} has been tentatively attributed to this direct-to-indirect crossover,³⁶ as a mirror-like description of the dichalcogenide case.^{8–10} However, the high effectiveness of the nanotexturing mechanism to enhance the luminescence response of even atomically thin InSe nanosheets is surprising on the basis of their indirect character. A similar direct-to-indirect crossover occurs in bulk InSe under pressure conditions.^{50–52} By increasing pressure, a ring-shaped valence band emerges and continuously develops, as shown by its effects on the hole concentration and mobility.⁵¹ However, this direct-to-indirect crossover, observed to appear in bulk InSe at 2 GPa, shows little effect on its intrinsic room-temperature PL until the pressure exceeds 4 GPa, when the difference between the direct and indirect band gaps is about 60 meV.^{50,52} In fact, pressure induced PL quenching in InSe is observed between 4 and 7 GPa, as a consequence of a second direct-to-indirect crossover in the conduction band along the ZB direction.⁵⁰ Taking into account that the difference between the direct and indirect band gaps is predicted to be few tens of meV in few layer InSe,^{35,49} the above-described facts indicate that the thermalization of holes among top valence band states tends to minimize the effects of the indirect nature of the nanosheets on their luminescence response at room temperature, suggesting that other processes different from the direct-to-indirect crossover are responsible for the PL quenching previously reported.^{35,36} Figure 4c shows the d dependence of the PL-peak integrated intensity of the spectra shown in Figure 4a. The wide d -range comprised in the present study allows to evidence that the reported strong quenching of the PL-signal^{35,36} is better described by a staggered reduction of the integrated PL intensity as d decreases, with a first quite abrupt step when d diminishes from 6.5 to 5 nm in which the PL intensity decreases by a factor ~ 5 followed by a more subtle step for d decreasing from 3 to 2 nm in which the PL intensity decreases

by a factor ~ 2 . This behavior of the integrated PL intensity points out quantum-size confinement effects acting on the optical properties of the 2D InSe layers not only through the progressive shift of the band gap as d decreases but also via the density of states available for optical absorption at each particular d . To illustrate these effects, we can consider that the PL peak intensity is mainly determined by the light absorption ratio, that can be evaluated as $1 - \exp(-\alpha d)$, where $\alpha = 2\pi \text{Im} \epsilon(\omega_{\text{exc}})/(n\lambda_{\text{exc}})$ is the InSe absorption coefficient at the incident-light energy (ω_{exc}), n is the refraction index, and λ_{exc} is the excitation light wavelength. The $\text{Im} \epsilon(\omega_{\text{exc}})$, the main contribution to the light absorption ratio, can be extracted from the data shown in Figure 3b taking into account that ω_{exc} was fixed to 2.54 eV in the experiments collected in Figure 4a. As quantum confinement effects are enhanced, different electron and hole sub-bands become involved in the optical absorption process, which makes $\text{Im} \epsilon(\omega_{\text{exc}} = 2.54 \text{ eV})$ to decrease by stages as d does (Figure 3b). For instance, optical absorption involves E_{g} - and E_{1} -related transitions in bulk InSe but E_{1} -related ones are no longer available for nanosheets thinner than ~ 5 nm. The light absorption ratio shown in Figure 4c has been calculated by using the obtained d dependence of the $\text{Im} \epsilon(\omega_{\text{exc}} = 2.54 \text{ eV})$, which predicts a negligible PL intensity for nanosheets thinner than 3 SLs that contrasts with observations. The relatively high luminescence response observed in these atomically thin nanosheets can be attributed to their unavoidable nanotexturized morphology, which is induced by the SiO_2 substrate. Apart from this, the calculated behavior of light absorption ratio appears to nicely account for the staggered behavior of the PL intensity observed with d , which also seems to indicate that the PL quantum yield is basically d -independent in spite of the large surface-to-volume ratio of the atomically thin nanosheets and suggests a negligible influence of defect-mediated nonradiative recombination processes as d decreases, that contrasts with the behavior observed in MoS_2 .⁵³

Results reported here on few-layer InSe widen the range of 2D materials with distinct and complementary optical properties to each other which have potential applications in optoelectronics. Particularly relevant is the huge band gap tuning of around 1 eV demonstrated in InSe as its thickness decreases from bulk to the SL. Nanotexturing—or, at its limit, important surface roughness effects—which usually induces undesirable phenomena as nonradiative recombination, has resulted to enhance the luminescent response of 2D InSe nanosheets. The evidenced ability of nanotexturing strategies to manipulate the optical response of 2D forms of InSe allows anticipating a robust and flexible property to be explored. The possibility that nanotexturing could be introduced in a controlled and scalable manner—by using patterned substrates, for instance—is particularly relevant for the potential applications of 2D InSe in photonics. These outstanding results also open the door for the design of high-performance flexible optoelectronic devices based on a 2D semiconductor which offers a wide optical window and can be eventually combined with other 2D semiconductors and graphene to obtain new semiconductor/semiconductor and metal/semiconductor heterostructures. Also, multiterraced 2D InSe devices, each terrace with a designed band gap, can serve to develop high-quality in-plane heterojunctions with minimal junction defect density due to the natural lattice match among terraces of different thicknesses.

Methods. InSe monocrystals used here to prepare the flakes were cleaved perpendicular to the (001) direction from an

ingot grown by the Bridgman method from a nonstoichiometric $\text{In}_{1.05}\text{Se}_{0.95}$ melt in which tin, in a content 0.01%, was introduced previously to growth to act as n-dopant. From these ingots, thin n-doped InSe samples were cleaved and used to prepare atomically thin InSe nanosheets on SiO_2/Si substrates by means of a mechanical exfoliation technique. The thickness of the SiO_2 layer was 300 nm. Morphology of the InSe nanosheets was measured by AFM, by using a Nanotec multimode microscope operating in contact mode for nanosheet thickness determination and in noncontact mode for studies focused on nanotexturing. Micro-PL measurements shown in Figure 4 were performed in air using Renishaw Invia micro-Raman system with 488 nm laser excitation, whereas those shown in Figures 1 and 2 were performed by using a Horiba Scientific Xplora micro-Raman system with 532 nm laser excitation. The optical beams were focused on the sample with a spot diameter of $\sim 2 \mu\text{m}$ and $\sim 1 \mu\text{m}$, respectively. A low laser power of $\sim 200 \mu\text{W}$ was used to prevent overheating.

The sol-gel method was used for the synthesis of ~ 100 nm silica nanoparticles by hydrolyzing tetraethylorthosilicate (TEOS) in a mixture of ethanol, water, ammonia, and surfactant. TEOS, ethanol, and ammonia were used as silica precursor, common solvent, and catalyst, respectively. Typically, 5.5 mL of ethanol, 11 mL of deionized water, and 0.8 mL of ammonia were mixed and stirred at 30°C . At the same time, a solution containing 5.5 mL of ethanol and 1.7 mL of TEOS is prepared and stirred at 30°C . Then, the latter is added to the first solution, and the reaction mixture is maintained at 30°C for 2 h. During this time, the reaction turns turbid slowly because of the formation of the silica NPs. Once the reaction is completed, 3-amino-propyltriethoxysilane (APS) is added dropwise to stabilize the particles. The resulting solution is heated at $80\text{--}90^\circ\text{C}$ to remove the excess of ammonia. The precipitate is collected by centrifugation and washed several times with water and ethanol and dried overnight at 100°C . Finally, the NPs are dispersed in water at a concentration of 1 g/L. SiO_2 NPs were deposited by spin-coating the aqueous solution at 1000 rpm onto the Si/SiO_2 substrates.

Calculations are based on density functional theory, using SIESTA code.⁵⁴ The exchange-correlation term is described by the local density approximation (LDA), with the functional form of Ceperley-Alder.⁵⁵ A numerical strictly localized double- ζ polarized basis set⁵⁶ is used to describe the valence electrons, while the core states are substituted by norm-conserving Troullier-Martins pseudopotentials.⁵⁷ Nonlinear partial core corrections to describe the exchange and correlations in the core region were included.⁵⁸ InSe finite multilayers were simulated using periodic slabs, including a large vacuum to avoid the interaction between periodic images. The calculations for the different slabs were carried out using the same geometrical details as for the bulk⁴⁸ since Rybkovskiy et al.⁵⁹ have recently shown that the geometrical variations between the bulk and different slabs of GaSe are not substantial. We have used a real-space grid equivalent to 1000 Ry plane-wave cutoff to describe the charge density and grids of $50 \times 50 \times 1$ and $30 \times 30 \times 30$ for the k -space according to the Monkhorst-Pack scheme⁶⁰ for the different slabs and bulk, respectively. We used the Fermi-Dirac distribution with an electronic temperature of 25 meV. Furthermore, a Gaussian broadening of 50 meV was included to plot the imaginary part of dielectric function for all multilayered cases, which was computed using the dipolar approximation using the density functional theory wave functions.

■ ASSOCIATED CONTENT

§ Supporting Information

The Supporting Information is available free of charge on the ACS Publications website at DOI: 10.1021/acs.nanolett.6b00689.

Further information on the nanotexturing process produced by the SiO_2 NPs on InSe nanosheets, electronic properties of 2D InSe nanosheets, angular dependence of the micro-PL in flat InSe nanosheets, and light scattering by SiO_2 NPs (PDF)

■ AUTHOR INFORMATION

Corresponding Authors

*E-mail (J.P.M.P.): Juan.Mtnez.Pastor@uv.es. Website: <http://www.uv.es/umdo>.

*E-mail (J.F.S.R.): Juan.F.Sanchez@uv.es. Website: <http://www.uv.es/lowdim>.

Notes

The authors declare no competing financial interest.

■ ACKNOWLEDGMENTS

This work was supported by the Spanish Government (Grant Nos. TEC2014-53727-C2-1-R and MAT2014-53500-R as well as Grants FIS2015-64886-C5-3-P and FIS2015-64886-C5-4-P), the Comunidad Valenciana Government (Grant No. PROMETEOII/2014/059), and the Generalitat de Catalunya Government (2014SGR301). The work at Berkeley was supported by National Science Foundation No. DMR-1306601. Authors thank the Central Support Service for Experimental Research (SCSIE) (SEM and Micro-PL facilities) of the University of Valencia. J.F.S.R. acknowledges financial support from the Mobility Program of VLC-CAMPUS. E.C., G.T., F.H., and P.O. acknowledge support of the Spanish MINECO through the Severo Ochoa Centers of Excellence Program under Grants SEV-2015-0496 and SEV-2013-0295. F.H. acknowledges support of CONACYT. M.B.G. acknowledges his fellowship no. UVINV-PREDOC13-110538 under the program "Atracció de Talent, VLC-CAMPUS" of the University of Valencia. D.A.P. acknowledges his contract CPI-15-276 under the program PROMETEOII/2014/059.

■ REFERENCES

- (1) Britnell, L.; Ribeiro, R. M.; Eckmann, A.; Jalil, R.; Belle, B. D.; Mishchenko, A.; Kim, Y.-J.; Gorbachev, R. V.; Georgiou, T.; Morozov, S. V.; Grigorenko, A. N.; Geim, A. K.; Casiraghi, C.; Castro Neto, A. H.; Novoselov, K. S. Strong light-matter interactions in heterostructures of atomically thin films. *Science* **2013**, *340*, 1311–1314.
- (2) Akinwande, D.; Petrone, N.; Hone, J. Two-dimensional flexible nanoelectronics. *Nat. Commun.* **2014**, *5*, 5678–5688.
- (3) Jariwala, D.; Sangwan, V. K.; Lauhon, L. J.; Marks, T. J.; Hersam, M. C. Emerging device applications for semiconducting two-dimensional transition metal dichalcogenides. *ACS Nano* **2014**, *8*, 1102–1120.
- (4) Lui, C. H.; Liu, L.; Mak, K. F.; Flynn, G. W.; Heinz, T. F. Ultraflat graphene. *Nature* **2009**, *462*, 339–341.
- (5) Dean, C. R.; Young, A. F.; Meric, I.; Lee, C.; Wang, L.; Sorgenfrei, S.; Watanabe, K.; Taniguchi, T.; Kim, P.; Shepard, K. L.; Hone, J. Boron nitride substrates for high-quality graphene electronics. *Nat. Nanotechnol.* **2010**, *5*, 722–726.
- (6) Jeong, S. Y.; Jeong, S.; Lee, S. W.; Kim, S. T.; Kim, D.; Jeong, H. J.; Han, J. T.; Baeg, K.-J.; Yang, S.; Jeong, M. S.; Lee, G.-W. Enhanced response and sensitivity of self-corrugated graphene sensors with anisotropic charge distribution. *Sci. Rep.* **2015**, *5*, 11216.

- (7) Lim, H.; Jung, J.; Ruoff, R. S.; Kim, Y. Structurally driven one-dimensional electron confinement in sub-5-nm graphene nanowrinkles. *Nat. Commun.* **2015**, *6*, 8601.
- (8) Mak, K. F.; Lee, C.; Hone, J.; Shan, J.; Heinz, T. F. Atomically thin MoS₂: A new direct-gap semiconductor. *Phys. Rev. Lett.* **2010**, *105*, 136805.
- (9) Splendiani, A.; Sun, L.; Zhang, Y. B.; Li, T. S.; Kim, J.; Chim, C. Y.; Galli, G.; Wang, F. Emerging photoluminescence in monolayer MoS₂. *Nano Lett.* **2010**, *10*, 1271–1275.
- (10) Tongay, S.; Zhou, J.; Ataca, C.; Lo, K.; Matthews, T. S.; Li, J.; Grossman, J. C.; Wu, J. Thermally driven crossover from indirect toward direct bandgap in 2D semiconductors: MoSe₂ versus MoS₂. *Nano Lett.* **2012**, *12*, 5576–5580.
- (11) Fang, H.; Chuang, S.; Chang, T. C.; Takei, K.; Takahashi, T.; Javey, A. High-performance single layered WSe₂ p-FETs with chemically doped contacts. *Nano Lett.* **2012**, *12*, 3788–3792.
- (12) Radisavljevic, B.; Radenovic, A.; Brivio, J.; Giacometti, V.; Kis, A. Single-layer MoS₂ transistors. *Nat. Nanotechnol.* **2011**, *6*, 147–150.
- (13) Lopez-Sanchez, O.; Lembke, D.; Kayci, M.; Radenovic, A.; Kis, A. Ultrasensitive photodetectors based on monolayer MoS₂. *Nat. Nanotechnol.* **2013**, *8*, 497–501.
- (14) Baugher, B. W. H.; Churchill, H. O. H.; Yang, Y.; Jarillo-Herrero, P. Optoelectronic devices based on electrically tunable p-n diodes in a monolayer dichalcogenide. *Nat. Nanotechnol.* **2014**, *9*, 262–267.
- (15) Perkins, F. K.; Friedman, A. L.; Cobas, E.; Campbell, P. M.; Jernigan, G. G.; Jonker, B. T. Chemical vapor sensing with monolayer MoS₂. *Nano Lett.* **2013**, *13*, 668–673.
- (16) Bernardi, M.; Palumbo, M.; Grossman, J. C. Extraordinary sunlight absorption and one nanometer thick photovoltaics using two-dimensional monolayer materials. *Nano Lett.* **2013**, *13*, 3664–3670.
- (17) Zhang, Y. J.; Oka, T.; Suzuki, R.; Ye, J. T.; Iwasa, Y. Electrically switchable chiral light-emitting transistor. *Science* **2014**, *344*, 725–728.
- (18) Mak, K. F.; McGill, K. L.; Park, J.; McEuen, P. L. The valley Hall effect in MoS₂ transistors. *Science* **2014**, *344*, 1489–1492.
- (19) Cappelluti, E.; Roldán, R.; Silva-Guillén, J. A.; Ordejón, P.; Guinea, F. Tight-binding model and direct-gap/indirect-gap transition in single-layer and multilayer MoS₂. *Phys. Rev. B: Condens. Matter Mater. Phys.* **2013**, *88*, 075409.
- (20) Liang, W. Y. Optical anisotropy in layer compounds. *J. Phys. C: Solid State Phys.* **1973**, *6*, 551–565.
- (21) Schuller, J. A.; Karaveli, S.; Schiros, T.; He, K.; Yang, S.; Kymissis, I.; Shan, J.; Zia, R. Orientation of luminescent excitons in layered nanomaterials. *Nat. Nanotechnol.* **2013**, *8*, 271–276.
- (22) Castellanos-Gomez, A.; Roldán, R.; Cappelluti, E.; Buscema, M.; Guinea, F.; van der Zant, H. S. J.; Steele, G. A. Local strain engineering in atomically thin MoS₂. *Nano Lett.* **2013**, *13*, 5361–5366.
- (23) Li, H.; Contryman, A. W.; Qian, X.; Ardakani, S. M.; Gong, Y.; Wang, X.; Weisse, J. M.; Lee, C. H.; Zhao, J.; Ajayan, P. M.; Li, J.; Manoharan, H. C.; Zheng, X. Optoelectronic crystal of artificial atoms in strain-textured molybdenum disulphide. *Nat. Commun.* **2015**, *6*, 7381.
- (24) Camassel, J.; Merle, P.; Mathieu, H.; Chevy, A. Excitonic absorption edge of indium selenide. *Phys. Rev. B: Condens. Matter Mater. Phys.* **1978**, *17*, 4718–4725.
- (25) Gomes da Costa, P.; Dandrea, R. G.; Wallis, R. F.; Balkanski, M. First-principles study of the electronic structure of γ -InSe and β -InSe. *Phys. Rev. B: Condens. Matter Mater. Phys.* **1993**, *48*, 14135–14141.
- (26) Brotons-Gisbert, M.; Sánchez-Royo, J. F.; Martínez-Pastor, J. P. Thickness identification of atomically thin InSe nanoflakes on SiO₂/Si substrates by optical contrast analysis. *Appl. Surf. Sci.* **2015**, *354*, 453–458.
- (27) Del Pozo-Zamudio, O.; Schwarz, S.; Klein, J.; Schofield, R. C.; Chekhovich, E. A.; Ceylan, O.; Margapoti, E.; Dmitriev, A. I.; Lashkarev, G. V.; Borisenko, D. N.; Kolesnikov, N. N.; Finley, J. J.; Tartakovskii, A. I. Photoluminescence and Raman investigation of stability of InSe and GaSe thin films. *arXiv:1506.05619*.
- (28) Segura, A.; Pomer, F.; Cantarero, A.; Krause, W.; Chevy, A. Electron scattering mechanisms in n-type indium selenide. *Phys. Rev. B: Condens. Matter Mater. Phys.* **1984**, *29*, 5708–5717.
- (29) Kress-Rogers, E.; Nicholas, R. J.; Portal, J. C.; Chevy, A. Cyclotron resonance studies on bulk and two-dimensional conduction electrons in InSe. *Solid State Commun.* **1982**, *44*, 379–383.
- (30) Martínez-Pastor, J.; Segura, A.; Valdes, J. L.; Chevy, A. Electrical and photovoltaic properties of indium-tin-oxide/p-InSe/Au solar cells. *J. Appl. Phys.* **1987**, *62*, 1477–1483.
- (31) Sánchez-Royo, J. F.; Segura, A.; Lang, O.; Pettenkofer, C.; Jaegermann, W.; Chevy, A.; Roa, L. Photovoltaic properties of indium selenide thin films prepared by van der Waals epitaxy. *Thin Solid Films* **1997**, *307*, 283–287.
- (32) Sánchez-Royo, J. F.; Segura, A.; Lang, O.; Schaar, E.; Pettenkofer, C.; Jaegermann, W.; Roa, L.; Chevy, A. Optical and photovoltaic properties of indium selenide thin films prepared by van der Waals epitaxy. *J. Appl. Phys.* **2001**, *90*, 2818–2823.
- (33) Julien, C.; Balkanski, M. Thin-film growth and structure for solid-state batteries. *Appl. Surf. Sci.* **1991**, *48–49*, 1–11.
- (34) Han, G.; Chen, Z.-G.; Drennan, J.; Zou, J. Indium selenides: structural characteristics, synthesis and their thermoelectric performances. *Small* **2014**, *10*, 2747–2765.
- (35) Sánchez-Royo, J. F.; Muñoz-Matutano, G.; Brotons-Gisbert, M.; Martínez-Pastor, J. P.; Segura, A.; Cantarero, A.; Mata, R.; Canet-Ferrer, J.; Tobias, G.; Canadell, E.; Marqués-Hueso, J.; Gerardot, B. D. Electronic structure, optical properties, and lattice dynamics in atomically thin indium selenide flakes. *Nano Res.* **2014**, *7*, 1556–1568.
- (36) Mudd, G. W.; Svatek, S. A.; Ren, T.; Patané, A.; Makarovskiy, O.; Eaves, L.; Beton, P. H.; Kovalyuk, Z. D.; Lashkarev, G. V.; Kudrynskiy, Z. R.; Dmitriev, A. I. Tuning the bandgap of exfoliated InSe nanosheets by quantum confinement. *Adv. Mater.* **2013**, *25*, 5714–5718.
- (37) Lei, S.; Wen, F.; Li, B.; Wang, Q.; Huang, Y.; Gong, Y.; He, Y.; Dong, P.; Bellah, J.; George, A.; Ge, L.; Lou, J.; Halas, N. J.; Vajtai, R.; Ajayan, P. M. Optoelectronic memory using two-dimensional materials. *Nano Lett.* **2015**, *15*, 259–265.
- (38) Sucharitakul, S.; Goble, N. J.; Kumar, U. R.; Sankar, R.; Bogorad, Z. A.; Chou, F.-C.; Chen, Y.-T.; Gao, X. P. A. Intrinsic electron mobility exceeding 10³ cm²/(Vs) in multilayer InSe FETs. *Nano Lett.* **2015**, *15*, 3815–3819.
- (39) Feng, W.; Zheng, W.; Cao, W.; Hu, P. Back gated multilayer InSe transistors with enhanced carrier mobilities via the suppression of carrier scattering from a dielectric interface. *Adv. Mater.* **2014**, *26*, 6587–6593.
- (40) Luo, W.; Cao, Y.; Hu, P.; Cai, K.; Feng, Q.; Yan, F.; Yan, T.; Zhang, X.; Wang, K. Gate tuning of high-performance InSe-based photodetectors using graphene electrodes. *Adv. Opt. Mater.* **2015**, *3*, 1418–1423.
- (41) Mudd, G. W.; Svatek, S. A.; Hague, L.; Makarovskiy, O.; Kudrynskiy, Z. R.; Mellor, C. J.; Beton, P. H.; Eaves, L.; Novoselov, K. S.; Kovalyuk, Z. D.; Vdovin, E. E.; Marsden, A. J.; Wilson, N. R.; Patané, A. High broad-band photoresponsivity of mechanically formed InSe–graphene van der Waals heterostructures. *Adv. Mater.* **2015**, *27*, 3760–3766.
- (42) Lei, S.; Wen, F.; Ge, L.; Najmaei, S.; George, A.; Gong, Y.; Gao, W.; Jin, Z.; Li, B.; Lou, J.; Kono, J.; Vajtai, R.; Ajayan, P.; Halas, N. J. An atomically layered InSe avalanche photodetector. *Nano Lett.* **2015**, *15*, 3048–3055.
- (43) Tamalampudi, S. R.; Lu, Y.-Y.; Kumar, U. R.; Sankar, R.; Liao, C.-D.; Moorthy, B. K.; Cheng, C.-H.; Chou, F. C.; Chen, Y.-T. High performance and bendable few-layered InSe photodetectors with broad spectral response. *Nano Lett.* **2014**, *14*, 2800–2806.
- (44) Yang, J.; Xu, R.; Pei, J.; Myint, Y. W.; Wang, F.; Wang, Z.; Zhang, S.; Yu, Z.; Lu, Y. Optical tuning of exciton and trion emissions in monolayer phosphorene. *Light: Sci. Appl.* **2015**, *4*, e312.
- (45) Bertolazzi, S.; Brivio, J.; Kis, A. Stretching and breaking of ultrathin MoS₂. *ACS Nano* **2011**, *5*, 9703–9709.

(46) Piccioli, N.; Le Toullec, R.; Chervin, J. C. Constantes optiques de InSe entre 10500 cm^{-1} (1,30 eV) et 22500 cm^{-1} (2,78 eV). *J. Phys. (Paris)* **1981**, *42*, 1129–1135.

(47) Lauth, J.; Gorris, F. E. S.; Khoshkhoo, M. S.; Chassé, T.; Friedrich, W.; Lebedeva, V.; Meyer, A.; Klinke, C.; Kornowski, A.; Scheele, M.; Weller, H. Solution-processed two-dimensional ultrathin InSe nanosheets. *Chem. Mater.* **2016**, *28*, 1728–1736.

(48) Rigoult, J.; Rimsky, A.; Kuhn, A. Refinement of the 3R γ -Indium monoselenide structure type. *Acta Crystallogr., Sect. B: Struct. Crystallogr. Cryst. Chem.* **1980**, *36*, 916–918.

(49) Debbichi, L.; Eriksson, O.; Lebègue, S. Two-dimensional indium selenides compounds: An *ab initio* study. *J. Phys. Chem. Lett.* **2015**, *6*, 3098–3103.

(50) Manjón, F. J.; Segura, A.; Muñoz-Sanjosé, V.; Tobias, G.; Ordejón, P.; Canadell, E. Band structure of indium selenide investigated by intrinsic photoluminescence under high pressure. *Phys. Rev. B: Condens. Matter Mater. Phys.* **2004**, *70*, 125201.

(51) Errandonea, D.; Segura, A.; Manjón, F. J.; Chevy, A.; Machado, E.; Tobias, G.; Ordejón, P.; Canadell, E. Crystal symmetry and pressure effects on the valence band structure of γ -InSe and ϵ -GaSe: Transport measurements and electronic structure calculations. *Phys. Rev. B: Condens. Matter Mater. Phys.* **2005**, *71*, 125206.

(52) Millot, M.; Broto, J. M.; George, S.; González, J.; Segura, A. Electronic structure of indium selenide probed by magnetoabsorption spectroscopy under high pressure. *Phys. Rev. B: Condens. Matter Mater. Phys.* **2010**, *81*, 205211.

(53) Amani, M.; Lien, D.-H.; Kiriya, D.; Xiao, J.; Azcatl, A.; Noh, J.; Madhvapathy, S. R.; Addou, R.; Kc, S.; Dubey, M.; Cho, K.; Wallace, R. M.; Lee, S.-C.; He, J.-H.; Ager, J. W.; Zhang, X.; Yablonovitch, E.; Javey, A. Near-unity photoluminescence quantum yield in MoS₂. *Science* **2015**, *350*, 1065–1068.

(54) Soler, J. M.; Artacho, E.; Gale, J. D.; García, A.; Junquera, J.; Ordejón, P.; Sánchez-Portal, D. The SIESTA method for *ab initio* order-*N* materials simulation. *J. Phys.: Condens. Matter* **2002**, *14*, 2745–2779.

(55) Perdew, J. P.; Zunger, A. Self-interaction correction to density-functional approximations for many-electron systems. *Phys. Rev. B: Condens. Matter Mater. Phys.* **1981**, *23*, 5048–5079.

(56) Junquera, J.; Paz, O.; Sánchez-Portal, D.; Artacho, E. Numerical atomic orbitals for linear-scaling calculations. *Phys. Rev. B: Condens. Matter Mater. Phys.* **2001**, *64*, 235111.

(57) Troullier, N.; Martins, J. L. Efficient pseudopotentials for plane-wave calculations. *Phys. Rev. B: Condens. Matter Mater. Phys.* **1991**, *43*, 1993–2006.

(58) Louie, S. G.; Froyen, S.; Cohen, M. L. Nonlinear ionic pseudopotentials in spin-density-functional calculations. *Phys. Rev. B: Condens. Matter Mater. Phys.* **1982**, *26*, 1738–1742.

(59) Rybkovskiy, D. V.; Arutyunyan, N. R.; Orekhov, A. S.; Gromchenko, I. A.; Vorobiev, I. V.; Osadchy, A. V.; Salaev, E.; Yu; Baykara, T. K.; Allakhverdiev, K. R.; Obraztsova, E. D. Size-induced effects in gallium selenide electronic structure: The influence of interlayer interactions. *Phys. Rev. B: Condens. Matter Mater. Phys.* **2011**, *84*, 085314.

(60) Monkhorst, H. J.; Pack, J. D. Special points for Brillouin zone integrations. *Phys. Rev. B* **1976**, *13*, 5188–5192.